Artículo de Investigación. Revista Ciencia e Ingeniería. Vol. 46, No. 3 pp. 303-312, agosto-noviembre, 2025.
ISSN 1316-7081. ISSN Elect. 2244-8780 Universidad de los Andes (ULA)

Syngas production and greenhouse gas mitigation using Fe/Ni bimetallic perovskite catalysts in methane dry reforming

Producción de gas de síntesis y mitigación de gases de efecto invernadero mediante catalizadores tipo perovskita Fe/Ni en el reformado seco de metano

Lugo, Claudio[1]*; Guerrero, Maryuri[1]; Fereira, Carla[1]; Petit, Eliel[1]; Torres, Ruben[1]; Vizcaya, Marietta[2]; Pérez, Patricia[2]; Rondón, Jairo[3]

[1]Laboratorio de Cinética y Catálisis, Departamento de Química, Facultad de Ciencias, Universidad de Los Andes, Mérida, Venezuela.
[2]Laboratorio de Polímeros, Departamento de Química, Facultad de Ciencias, Universidad de Los Andes, Mérida, Venezuela.
[3]Biomedical & Chemical Engineering Departments, Universidad Politécnica de Puerto Rico, San Juan, Puerto Rico, USA.

**claudiolugo@ula.ve*

Abstract

In this investigation, mixed oxides of the perovskite type with formula $Ba_{0,3}Sr_{0,7}Ni_{1-x}Fe_xO_3$ (x = 0,0-0,3-0,5-0,7-1,0) were synthesized via solution combustion, SCS, in the presence of microwave radiation. The oxides were characterized by Fourier transform infrared spectroscopy, FTIR, and X-ray diffraction, XRD. The spectroscopic study shows distinctive signals of M-O interactions at low wavelengths. X-ray diffraction allowed the identification of the primary phase present, an orthorhombic perovskite (space group: Pnma) of the $LaFe_{0.6}Ni_{0.4}O_3$ type, formed during the combustion of glycine; this technique allowed the calculation of the size of the crystalline domain, with values below 20 nm for all perovskites. The catalytic performance for the dry reforming reaction of methane with perovskites as catalysts shows good thermal stability and resistance to sintering and deactivation by carbon deposition. The perovskites with the highest average methane conversion were NiFe-MG3 and NiFe-MG4 with 87,54 and 61,14 % hydrocarbon conversion, respectively.

Keywords: *Perovskites, mixed oxides, methane reforming, greenhouse gases.*

Resumen

En esta investigación se sintetizaron óxidos mixtos tipo perovskitas de fórmula $Ba_{0,3}Sr_{0,7}Ni_{1-x}Fe_xO_3$ (x = 0,0-0,3-0,5-0,7-1,0) vía combustión en solución, SCS, en presencia de radiación microondas. Los óxidos se caracterizaron a partir de la espectroscopia infrarroja con transformada de Fourier, FTIR y la difracción de rayos x, DRX. El estudio espectroscópico muestra señales distintivas de las interacciones M-O a longitudes de onda bajas. La difracción de rayos x permitió identificar como fase principal presente, una perovskita ortorrómbica (grupo espacial: Pnma) tipo $LaFe_{0,6}Ni_{0,4}O_3$, formada durante la combustión de la glicina; esta técnica permitió calcular el tamaño del dominio cristalino, con valores por debajo de los 20 nm para todas las perovskitas. El performance catalítico para la reacción de reformado seco de metano con las perovskitas como catalizadores de la reacción, muestra buena estabilidad térmica y resistencia a la sinterización y desactivación por deposición de carbono. Las Perovskitas con mayor conversión promedio de metano fueron NiFe-MG3 y NiFe-MG4 con un 87,54 y 61,14 % de conversión del hidrocarburo respectivamente.

Palabras clave*: Perovskitas, óxidos mixtos, reformado de metano, gases de invernadero.*

1 Introduction

Since the Industrial Revolution in the mid-18th century, humanity has undergone profound transformations in economic, social, cultural, and technological spheres, leading to changes in the number, type, and distribution of living species. This is mainly due to the exploitation of natural resources, indiscriminate soil plowing, and pollution of the atmosphere, seas, and oceans, all contributing to the progressive deterioration of planet Earth (Kammer et al., 2001; Arevalo, 2019).

In recent years, mixed oxides have been studied for use as heterogeneous catalysts in industrial processes. Their popularity is growing due to significant advantages over other types of catalysts, such as lower energy consumption and reduced harmful environmental effects. Various methods have been developed for their preparation based on their crystallographic (surface-to-volume ratio) and

electronic properties relevant to catalysis. Among them, solution combustion synthesis (SCS) stands out as a rapid technique that does not require expensive equipment and starts from metal precursor salts (Civera et al., 2003; Specchia et al., 2004; Wang et al., 2009; García et al., 2010; Pérez et al., 2015; Lugo et al., 2010-2022-2024.a).

Certain mixed oxides, such as perovskites, exhibit ideal properties for use as catalysts in heterogeneous processes like methane reforming. SCS enables the synthesis of nanoparticles with unique properties compared to their bulk counterparts. These materials also promote the formation of synthesis gas (a mixture of CO and H_2) while minimizing coke deposition, one of the leading causes of active site deactivation in catalysts (Lugo et al., 2010).

Part of the produced synthesis gas (syngas) is used for electricity generation, particularly through Integrated Gasification Combined Cycle (IGCC) technology. Although syngas can be derived from almost any carbon-rich source, such as oil, coal, biomass, or organic waste, natural gas is the primary feedstock for syngas production. Moreover, the abundance of this raw material makes methane reforming a feasible process for obtaining syngas (Edwards et al., 1995; Cabrera et al., 2012).

Natural gas (an abundant resource in Venezuela) is primarily a mixture of gases, with methane accounting for 75% to 95% of the total volume. Other components include ethane, propane, butane, nitrogen, carbon dioxide, hydrogen sulfide, helium, and argon (Wang et al., 2009). Venezuela holds the tenth-largest proven natural gas reserves globally (~5.67 trillion cubic meters), much of which is associated gas (C.I.A., 2021).

The average composition of Venezuelan natural gas is approximately 82% methane (CH_4), 10% ethane (C_2H_6), 3.7% propane (C_3H_8), and 0.2% carbon dioxide (CO_2). The final product is mainly methane, with a small fraction of ethane. Much of this methane is flared and released into the atmosphere, leading to economic losses for the nation and negative environmental impacts (García, 2012).

Supported catalysts based on transition metals as the active phase (metal oxide or metal) can form a dispersed phase on a high-surface-area support, which enhances catalytic activity and stability. Metals, metal oxides, metal sulfides, organometallic complexes, and enzymes can be supported on inorganic solids such as metal oxides, zeolites (aluminosilicates), or clays. In these catalysts, the active phase typically appears as nanometer-sized crystals (10^{-9} m = 1 *nm*). Additionally, a wide range of metal oxide-based catalysts is available for various commercial processes (Martín et al., 2021).

This work prepared bimetallic perovskites (Fe/Ni) using solution combustion synthesis (SCS). The solids were characterized by Fourier-transform infrared spectroscopy (FTIR) and X-ray diffraction (XRD). Catalytic testing was performed by coupling a gas chromatograph (GC) to the reaction system. The perovskites were used as catalysts for the dry reforming of methane (DRM), and the results demonstrate that these materials (perovskite oxides) are suitable for this type of reaction due to their high thermal stability and hydrocarbon activation capability.

2 Experimental procedure

2.1 Synthesis of perovskites

The mixed oxides were prepared using solution combustion synthesis (SCS), as described by Patil (Patil et al., 1997–2002), Mukasyan (Mukasyan et al., 2001–2007), and Varma (Varma et al., 2003), and verified at the Kinetics and Catalysis Laboratory of the Universidad de Los Andes by Pérez (Pérez et al., 2015), Briceño (Briceño et al., 2020), and Lugo (Lugo et al., 2010–2017–2022–2024a–2024b).

2.1.1 Synthesis methodology

Once the precursor mixture was prepared, it was placed in a modified porcelain crucible with a lid to allow the release of gases produced during fuel combustion. The crucible was then placed in a domestic microwave oven (Premium brand, model PM7078, 700W power), and radiation was applied at 80% of maximum power (Zhao et al., 2004).

Combustion of the precursor mixture occurred after 35 seconds of irradiation. It continued for approximately 15 more seconds, during which violent flames and a large amount of gas were generated due to the ionization of gases accumulated inside the ceramic trap, further increasing the temperature inside the crucible. The total irradiation time of the precursor mixture was approximately 95 seconds. At the end of the process, a fine grayish powder was obtained, corresponding to the perovskite-type mixed oxide.

2.1.2 Stoichiometry

The different perovskites synthesized via SCS are shown in Table 1. Additionally, the starting material, gel formation, and the solid synthesized with and without maceration-obtained after the combustion of the precursor mixture-can be observed in Figure 1.

Table 1. Perovskite-type compounds $Ba_{0,3}Sr_{0,7}Ni_{1-x}Fe_xO_3$ (x= 0,0-0,3-0,5-0,7-1,0) synthesized via SCS.

Formula (ABO_3)	Ignition	Code
$Ba_{0,3}Sr_{0,7}FeO_3$	Microwave	Fe-MG-1
$Ba_{0,3}Sr_{0,7}Ni_{0,3}Fe_{0,7}O_3$		NiFe-MG-2
$Ba_{0,3}Sr_{0,7}Ni_{0,5}Fe_{0,5}O_3$		NiFe-MG-3
$Ba_{0,3}Sr_{0,7}Ni_{0,7}Fe_{0,3}O_3$		NiFe-MG-4
$Ba_{0,3}Sr_{0,7}NiO_3$		Ni-MG-5

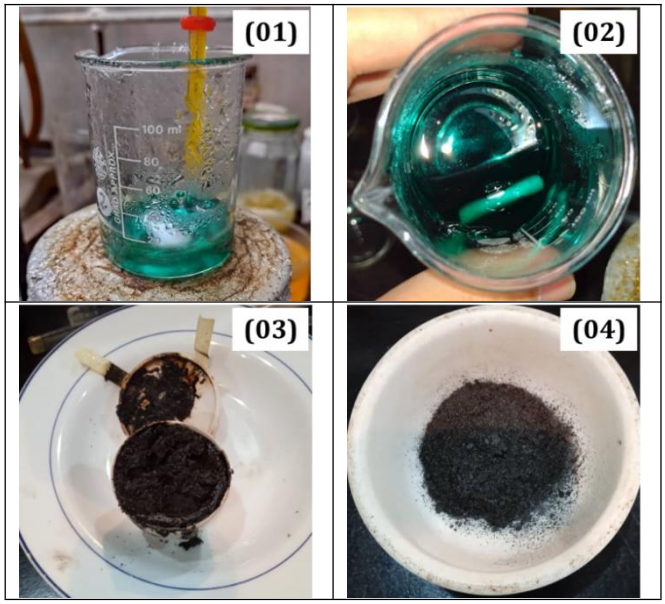

Figure 1. SCS synthesis of *Perovskites*: 1.- Start of SCS, 2.- Gel formation (before irradiation), 3.- Product after microwave irradiation, MO, and 4.- Maceration.

2.2 Characterization

The synthesized materials were characterized by:

1. Fourier-transform infrared spectroscopy (FTIR), using a Perkin Elmer Frontier FTIR Spectrophotometer, and

2. X-ray diffraction (XRD) in powder form, using a Bruker D8 Advance diffractometer with Cu Kα radiation (wavelength 1.5406 Å), operating at 40 kV and 40 mA. Data were recorded in the 2θ range of 2°–70°, with a step time of 0.6 s and a step size of 0.02035°.

3. Results and discussion

3.1 Fourier-transform infrared spectroscopy (FTIR)

The infrared spectra of the perovskites of the type $Ba_{0,3}Sr_{0,7}Ni_{1-x}Fe_xO_3$ (x = 0,0-0,3-0,5-0,7-1,0), synthesized via SCS, are shown in Figure 2. Table 2 presents the band assignments of the infrared spectrum for the synthesized solids. The band at 3401.5 cm^{-1} corresponds to symmetric and asymmetric stretching vibrations of the O–H group, related to water molecules coordinated in the solids, originating from the synthesis process (Ramos et al., 2015; Neira et al., 2016). At 2925 and 2854 cm^{-1}, two low-intensity peaks are observed, attributed to the $–CH_2–C=O$ stretching vibrations with sp^3 hybridization, resulting from excess fuel during synthesis (Wade, 2004). The signal around 1625.7 cm^{-1} is due to an asymmetric deformation of the carboxylate ion (COO^-), a species formed during synthesis (Hernández et al., 2006). A band near 1450.8 cm^{-1} is associated with asymmetric stretching vibrations of nitrate groups (NO_3^-) from the synthesis and/or atmospheric carbonate (CO_3^{2-}) absorption (Darroudia et al., 2016; Song et al., 2016).

The peak at approximately 1384 cm^{-1} corresponds to symmetric stretching vibration of the N–O bond (NO_2 type species), associated with bidentate coordination compounds (Rendón et al., 2006). The signal at 1091.6 cm^{-1} is attributed to in-plane bending modes of the C–O bond, associated with acetals and saturated primary aliphatic alcohols. The band at 1024.5 cm^{-1} results from out-of-plane bending of the C–H bond, present in all precursors, and provides information about the NH_4OH added during synthesis to adjust the pH (Gómez, 2010).

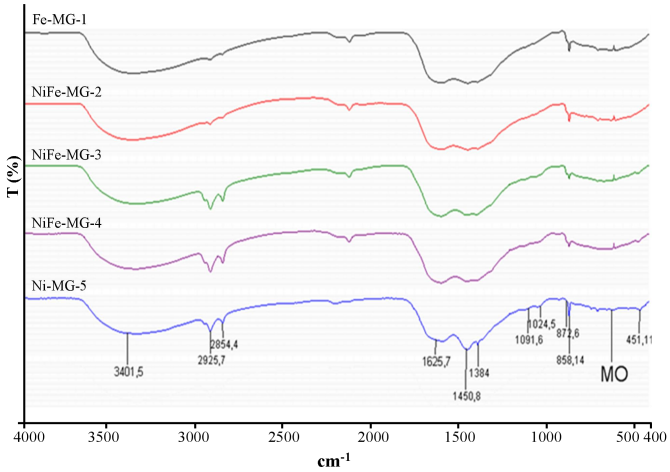

Figure 2. FTIR spectra of the synthesized perovskite-type (Fe/Ni) oxides.

There is a region known as the *fingerprint region* of metal–oxygen (M–O) interactions (at lower wavelengths), where characteristic signals of the vibrational modes permitted for metals and non-metals (Fe^{2+}, Ni^{2+}, Sr^{2+}, and Ba^{2+}) can be observed, involving OH groups and oxygen atoms bonded to these metals (O–M–O) (Anacona et al., 2013).

At 872.6 cm^{-1}, a peak appears corresponding to the bending vibration of the Sr–O bond in an octahedral site (Sithole et al., 2017; Briceño et al., 2020). Near 858.14 cm^{-1}, a band is associated with stretching vibrations of the Ba–O bond (Villaquirán et al., 2015). The signal at 640 cm^{-1} is attributed to the characteristic stretching vibration of the Sr–O bond (Harish et al., 2017). The peak around 630 cm^{-1} may be associated with vibrations of the face-centered cubic Ni–O phase (Liu et al., 2013).

Near 600 cm^{-1}, bending vibrations of the Fe–O bond are observed, corresponding to the MO_6 octahedral structure. The intensity of this signal decreases as the degree of iron substitution increases (Haye et al., 2017).

Table 2. Band assignments of FTIR spectra for (Fe/Ni) perovskites.

v (Ref.) cm^{-1}	v (cm^{-1})	Bond	Assignment
3440	3401,5	O–H	Symmetric and asymmetric stretching vibrations of the O–H group.
3050-2870	2925-2854	CH_2–C=O	–CH_2–C=O stretching vibrations.
1650-30	1625,7	COO–M	Asymmetric deformation of the carboxylate ion (COO^-–M).
1470-40	1450,8	N–O/C–O	Asymmetric stretching vibrations of nitrate (NO_3^-) and/or carbonate (CO_3^{2-}) groups.
1384	1384	N–O	Symmetric stretching of NO_2 (N–O bond).
1040	1091,6	C–O	In-plane bending modes of the C–O bond.
1025	1024,5	C–H	Out-of-plane bending of the C–H bond.
Metal–Oxygen Interactions			
862	872,6	Sr–O	Bending vibrations of the Sr–O bond in an octahedral site.
864	858,14	Ba–O	Stretching vibration of the Ba–O bond.
660	~640	Sr–O	Stretching vibration of the Sr–O bond.
660	~630	Ni–O	Ni–O bond vibrations in a face-centered cubic structure.
558	~600	Fe–O	Bending vibrations of the Fe–O bond in the MO_6 octahedral structure.
470	~451	Ni–O	Ni–O bond vibration.

Finally, the peak at 451 cm^{-1}, located at a low wavenumber, is attributed to asymmetric vibrations of the Ni–O bond (Rahdar et al., 2015).

3.2 X-ray diffraction (XRD)

Figure 3 shows the XRD patterns of the perovskites $Ba_{0,3}Sr_{0,7}Ni_{1-x}Fe_xO_3$ (x = 0,0 - 0,3 - 0,5 - 0,7 - 1,0). Phase identification of the synthesized materials was carried out using the X'Pert HighScore Plus 2.1 software with the PDF2-2004 database from the ICDD.

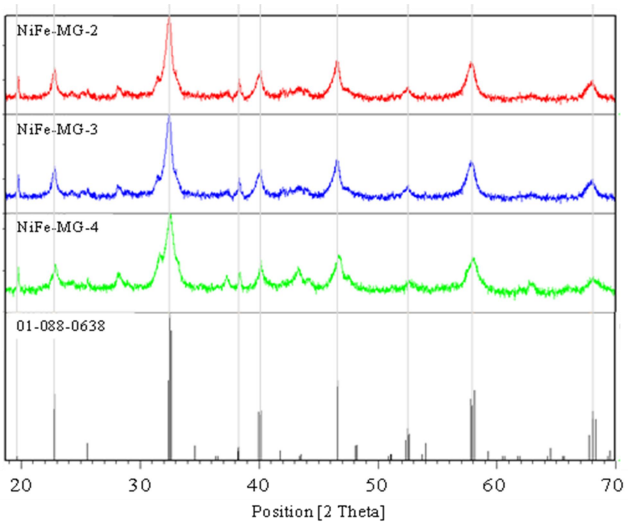

Figure 3. X-ray diffraction patterns of the $Ba_{0,3}Sr_{0,7}Ni_{1-x}Fe_xO_3$.perovskites. Reference: 01-070-1333 (perovskite La_2NiO_4).

The presence of an orthorhombic perovskite-type phase (space group: Pnma), specifically lanthanum iron-nickel oxide, $LaFe_{0,6}Ni_{0,4}O_3$, was identified, matching the reference card 01-088-0638 (Falcon et al., 1990).

The formation of the perovskite phase is favored in the prepared solids due to the extremely high temperatures reached during the combustion process, which promotes the crystallization of the perovskite phase (Pérez et al., 2015).

3.2.1 Crystallite size calculation

The crystallite size of the synthesized oxides was calculated using the Scherrer equation (Eq. 01) (Langford et al., 1978).

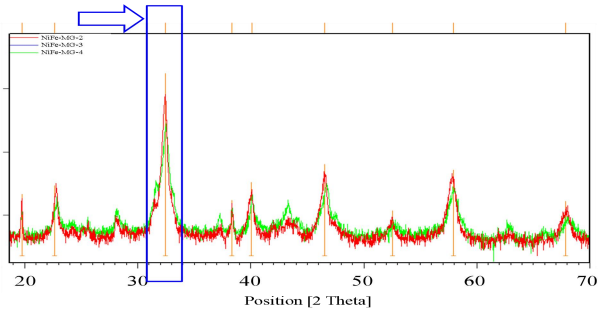

Figure 4. Diffraction pattern showing the hkl (103) line used to calculate the crystallite domain size of the perovskite.

$$\beta = \frac{(0.89).\lambda}{FWHM_{(S)}.(\cos 2\theta)} \quad \text{(Eq. 01)}$$

β = crystallite domain size.
λ = wavelength of the radiation used (λ_Cu) in nm.
FWHM(S) = full width at half maximum of the diffraction peak at angle θ.

$$FWHM(S) = \frac{SF\ x\ A}{l} \quad \text{(Eq. 02)}$$

SF = shape factor constant, approximately 0.85.
A = sum of the net intensity of all points forming the diffraction peak.
l = height of the diffraction peak at angle θ.

In all cases, the (103) diffraction line was selected, corresponding to the most intense peak of the dominant phase in the synthesized oxides (Fig. 4).

Table 3 presents the crystallite domain sizes determined using the Scherrer equation (Eq. 01–02). It can be observed that the prepared solids exhibit average crystallite domain sizes below the threshold commonly used to classify them as nanoparticles—that is, diameters smaller than 20 *nm*.

Table 3. Parameters used and diameters of the crystalline domain of *Perovskites*.

Código	SF	Área	Altura	k	λ (Cu)	2θ	cos2θ	FWHM(S)	*d(nm)*
NiFe-MG-2	0,85	352,7	1017,9	1,00	1,54	32,46	0.5027	0,51980	**5,89**
				0,89		32,46	0.5027	0,29455	**9,26**
NiFe-MG-3	0,85	190,3	1023,1	1,00	1,54	32,43	0.5263	0,27910	**10,48**
				0,89		32,43	0.5263	0,15815	**16,47**
NiFe-MG-4	0,85	335,1	666,6	1,00	1,54	32,53	0.4365	0,75420	**4,68**
				0,89		32,53	0.4365	0,42737	**7,35**

3.3 Catalytic test: Dry reforming of methane

3.3.1 Instrumental response (gas chromatograph – GC)

For the gas chromatograph, the thermal conductivity detector's (TCD) response factor was calculated using argon as the carrier gas, flowing at a rate of 30 *mL/min* through the internal column system.

Table 4. TCD response factors for each gas.

Gaseous compound	TCD Response Factor
Hydrogen	8.29
Methane	3.76
Carbon dioxide	1.26
Carbon monoxide	1.00

**All values relative to CO.*

The GC oven was operated under isothermal conditions at approximately 150°*C*. A distinct response factor was verified for each compound (Table 4).

3.3.2 Pretreatment

The synthesized (Fe/Ni) perovskites were pretreated with hydrogen at a 30 *mL/min* flow rate, using a heating ramp programmed to increase at 10 °*C/min* from room temperature to 700 °*C*. The temperature was held at 700 °*C* for approximately 15 minutes (Fig. 5).

3.3.3 Calibration (gas chromatograph – GC)

Parameters such as mass, reactant flow rate, temperature range, and space velocity were calibrated to ensure kinetic regime conditions during the reaction. The ideal conditions for kinetic studies using perovskites in the DRM (Dry Reforming of Methane) system are summarized in Table 5.

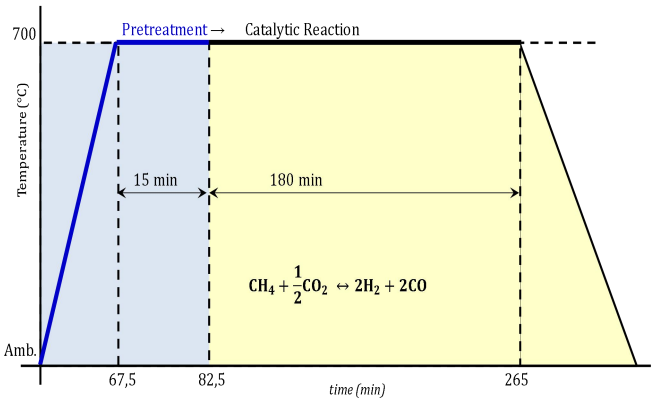

Figure 5. Thermal cycle (pretreatment/catalytic reaction) in DRM using perovskites as catalysts.

Table 5. Actual conditions used for GC analysis.

Parameter	Value
Total flow rate (*mL/min*)	≥ 50
Temperature range (°*C*)	700
Catalyst mass (mg)	≥ 0.030
Space velocity range ×10^{-3} (*mL/g*h*)	120–240

3.3.4 Reaction conditions

Approximately 30 *mg* of perovskite catalyst was weighed and placed into a U-shaped quartz reactor. The reaction temperature was set to 700 °*C*. The molar feed ratio of the reactants CH_4/CO_2 was 1:1, with a total volumetric flow rate of 40 *mL* and a space velocity of 120.000 *mL/g*h*.

3.3.5 Catalytic test (methane reforming)

The conversions of methane and carbon dioxide, the selectivity towards synthesis gas, and the H_2/CO molar ratio for the DRM reaction using $Ba_{0,3}Sr_{0,7}Ni_{1-x}Fe_xO_3$ perovskites as heterogeneous catalysts at 700 °C are shown in Figure 6. It was found that the partial substitution of iron with nickel

enhances both the activity and selectivity of the dry reforming of methane to synthesis gas. All perovskite catalysts tested in the DRM reaction exhibited good thermal stability over a reaction time of approximately 200 minutes, indicating resistance to sintering and minimal deactivation due to carbon deposition.

The stability observed in the DRM reaction may be related to: 1) the small size of the metallic particles, particularly the average size of nickel, and 2) The strong interaction of the metallic sites with the support structure at high temperatures (Sierra et al., 2009; García et al., 2010).

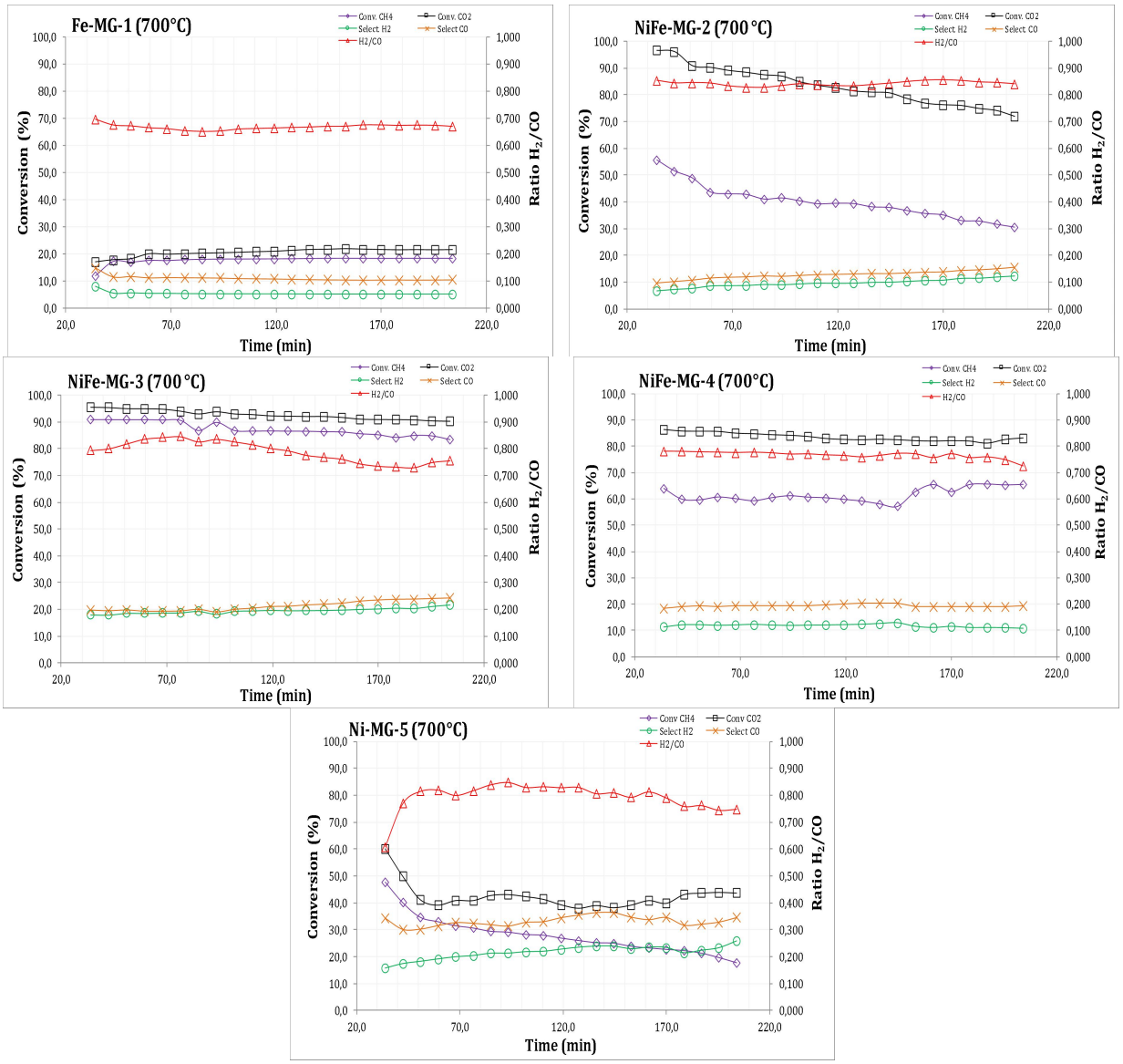

Figure 6. CH_4 and CO_2 conversions, *Syngas* selectivity, and H_2/CO ratio for $Ba_{0,3}Sr_{0,7}Ni_{1-x}Fe_xO_3$ perovskites in the DRM reaction.

Table 6. Average conversions (%) of CH_4 and CO_2, H_2/CO ratio, and selectivity towards syngas for the perovskites at 700 °C.

Measured Parameter	Fe-MG-1	NiFe-MG-2	NiFe-MG-3	NiFe-MG-4	Ni-MG-5
CH_4 Conversion (%)	17,78	39,97	87,54	61,14	27,93
CO_2 Conversion (%)	20,56	83,28	92,70	83,63	42,45
H_2/CO Ratio	0,67	0,84	0,79	0,77	0,79
H_2 Selectivity (%)	5,28	9,66	19,39	11,93	21,56
CO Selectivity (%)	11,01	12,69	21,15	19,52	33,20
Σ Selectivity (H_2 + CO) (%)	16,28	22,35	40,54	31,45	54,76

The conversion of carbon dioxide is favored over methane in all solids of the P-NiCo-RT series, due to the presence of simultaneous competitive reactions such as the reverse water–gas shift reaction (RWGS), where CO_2 reacts with H_2 to produce CO and water vapor (Haghighi et al., 2007) (Eq. 03).

$$CO + H_2O \leftrightarrows CO_2 + H_2 \qquad \Delta H^\circ \; +9{,}8 \; Kcal/mol \qquad \text{(Eq. 03)}$$

The H_2/CO molar ratio showed values below 1, which is likely due to side reactions such as the reverse water–gas shift reaction (Eq. 03), resulting in increased CO and consequently a lower final H_2/CO ratio, deviating from the stoichiometry of the DRM reaction (Lugo et al., 2010). The relatively low selectivity percentages may be attributed to the extreme operating conditions and secondary reactions competing for the active metal sites.

Among the $Ba_{0,3}Sr_{0,7}Ni_{1-x}Fe_xO_3$ perovskite catalysts tested at 700 °*C*, the highest CH_4 conversions were observed for:

(NiFe-MG-3)		(NiFe-MG-4)
87,37 %	>	61,62 %

The observed catalytic pathway is attributed to a **synergistic effect** between iron and nickel, which appears to enhance the properties of the metallic active sites.

4 Conclusions

Mixed oxide perovskite-type materials were successfully synthesized via solution combustion synthesis (SCS)—a rapid, efficient, and cost-effective method for obtaining nanomaterials.

FTIR spectroscopy confirmed the presence of characteristic vibrational modes of metal–oxygen interactions at low wavenumbers (<1000 cm^{-1}), revealing overlapping bands indicative of the presence of these metals in the synthesized heterogeneous catalyst.

XRD patterns of the bimetallic samples (NiFe-MG2, NiFe-MG3, NiFe-MG4) revealed the formation of a dominant orthorhombic perovskite-type phase (space group: *Pnma*) corresponding to lanthanum iron-nickel oxide, $LaFe_{0.6}Ni_{0.4}O_3$, identified using reference card 01-088-0638 from the ICDD PDF2-2004 database.

Crystallite domain size estimation using the Scherrer equation indicated particle sizes below 20 *nm*, confirming the presence of nanoparticles in the material structure.

Catalytic tests for DRM demonstrated that partial iron substitution with nickel enhances activity and selectivity toward synthesis gas. Most perovskites exhibited good thermal stability over the reaction duration, indicating resistance to sintering and minimal deactivation from carbon deposition.

Average methane conversions in DRM for the synthesized perovskites were as follows:

NiFe-MG-3	>	NiFe-MG-4	>	NiFe-MG-2
(87,54 %)		(61,14 %)		(39,97 %)

This supports a synergistic effect between Ni and Fe that improves active site performance, resulting in higher hydrocarbon conversions.

CO_2 conversion was favored in the reaction system, likely due to competitive secondary reactions such as the reverse water–gas shift reaction, where CO_2 reacts with H_2 to form CO and water.

All H_2/CO molar ratios in the DRM reaction were below unity, confirming the presence of the RWGS reaction, which increases CO production and thus decreases the final H_2/CO ratio in the syngas mixture.

Acknowledgments

We thank the X-ray Laboratory of the Universidad Industrial de Santander and its director, Professor José Antonio Henao Martínez, for his invaluable support in the powder X-ray diffraction analyses of the synthesized samples in this study.

References

Anacona, O., García, D., Kiminami, R. y Raigoza, C., (**2013**). Efecto de la temperatura en la estructura cristalina de polvos cerámicos de $K_{0.5}Na_{0.5}NbO_3$ obtenidos por el método de reacción por combustión, Revista latinoamericana de Metalurgia y Materiales, Vol. 33 (1), pp. 108-115.

Arévalo, R., (**2019**). La Industria y sus efectos en el cambio climático Global. RECIAMUC, Vol. 2 (2), pp. 595-611.

Briceño, J., Lugo, C., García, E., Rondón, J., Pérez, P., Rodríguez, P., Del Castillo, H. y Imbert, F., (**2020**). Síntesis de perovskitas basadas en Ni y Fe vía SCS con radiación microondas y su empleo en el reformado seco de metano. Revista Ciencia e Ingeniería, Vol. 41 (2), pp. 205-216.

Cabrera, G., Madriñan, S., Muñoz, D., (**2012**). Caracterización del gas de síntesis obtenido a partir de algarrobo y bagazo de caña. Biotecnología en el Sector Agropecuario y Agroindustria, Vol. 10 (1), pp. 166-172.

C.I.A., (**2021**). Natural gas - proved reserves. The World Factbook. https://www.cia.gov/the-world-factbook/static/3a6e5fc200e47bc5cf68bd3a5d57481b/Energy_World.pdf

Civera, A., Pavese, M., Saracco, G. y Specchia, V., (**2003**). Combustion synthesis of perovskite-type catalysts for

natural gas combustion. Catalysis Today, Vol. 83, pp. 199-211.

Darroudia, M., Bagherpour, M., Hosseini, H. y Ebrahimic, M., (**2016**). Biopolymer-assisted green synthesis and characterization of calcium hydroxide nanoparticles. Ceramics International, Vol. 42 (3), pp. 3816-3819.

Edwards, J. y Maitra, A., (**1995**). The chemistry of methane reforming with carbon dioxide and its current and potential applications. Fuel Processing Technology, Vol. 42 (2-3), pp. 269-289.

Falcon, H., Goeta, A., Punte, G., Carbonio, R., (**1997**). Crystal structure refinement and stability of $LaFe_xNi_{1-x}O_3$ solid solutions, Journal of Solid State Chemistry, Vol. 133(2), pp. 379-385.

García, F., (**2012**). Estimación técnico económica de la separación de los compuestos de gas licuado de petróleo a partir de gases de quema y/o venteo. Trabajo Especial de Grado, Facultad de Ingeniería, Universidad Central de Venezuela, pp. 10-24.

García, E., Rondón, J., Belandria, L., Meléndez, H., Lugo, C. y Imbert F., (**2010**). Dry methane reforming over Ni-Co supported by impregnation on MgO nanoparticles, Revista Ciencia e Ingeniería, Vol. 31 (2), pp. 77-82.

Gómez, J., (**2010**). Síntesis y caracterización del sistema $LaSrCrFeO_3$ soportado sobre óxidos de cerio dopados con elementos de transición interna. Tesis Doctoral en Ciencias Química, Departamento de Química, Facultad de Ciencias, Universidad Nacional de Colombia, Bogotá, Colombia, pp. 156-158.

Haghighi M., Sun Z., Wu J., Bromly J., Wee H.L., Ng E., Wang Y., Zhang D., (**2007**). On the reaction mechanism of CO_2 reforming of methane over a bed of coal char, Proceedings of the Combustion Institute, Vol. 31 (2), pp. 1983-1990.

Harish, S., Sabarinathan, M., Archana, J., Navaneethan, M., Nisha, K., Ponnusamy, S., Gupta, V., Muthamizhchelvan, C., Aswal, D., Ikeda, H., Hayakawa, Y., (**2017**). Synthesis of ZnO/SrO nanocomposites for enhanced photocatalytic activity under visible light irradiation, Applied Surface Science, Vol. 418(A), pp. 147-155.

Haye, E., Bruyere, S., André, E., Boulet, P., Barrat, S., Capon, F., Miska, P., Migot, S., Carteret, C., Coustel, R., Gendarme, C., Diliberto, S., Munnik, F., (**2017**). $LaFeO_xN_y$ perovskite thin films: Nitrogen location and its effect on morphological, optical and structural properties. Journal of Alloys and Compounds, Vol. 724, pp. 74-83.

Hernández, J., Castillo, S., Esparza, H., Téllez, E. y Duarte, J., (**2006**). Síntesis y caracterización de nano-monocristales de Glicina-Nitrato de Sodio, GSN, con propiedades ópticas no-lineales. Tecnura, Vol. 9 (18), pp. 4-9.

Kammer, K., Skou, E., Christensen, H., Turek, T., (**2001**). Perovskites as Catalysts for the Selective Catalytic GaoReduction of Nitric Oxide with Propene: Relationship between Solid State Properties and Catalytic Activity. Journal of Catalysis, Vol. 199 (1), pp. 32-140.

Langford, J. y Wilson, A., (**1978**). Scherrer after sixty years: A survey and new results in determining crystallite size. Journal of Applied Crystallography, Vol. 11, pp. 102-113.

Liu, L., Guo, Y., Wang, Y., Guo, H., (**2013**). Hollow NiO nanotubes synthesized by bio-templates as the high-performance anode materials of lithium-ion batteries. Electrochimica Acta, Vol. 114, pp. 42-47

Lugo, C., García, E., Rondón, J., Meléndez, H., Pérez, P. y Del Castillo, H., (**2010**). Síntesis de óxidos mixtos de Co, Ni y Cu sobre MgO por el método de combustión con urea y estudio en la reacción de reformado seco de metano con CO_2. Revista Ciencia e Ingeniería, Vol. 31 (1), pp. 53-60.

Lugo, C., Pérez, M., Quintero, M., Rondón, J., Pérez, P., D´Angelo, R., Meléndez, H., Villarroel, M., Rodríguez, P., Imbert, F. y Del Castillo, H., (**2017**). Study of the reaction of dry reforming of methane using mixed oxide perovskites type $La_xSr_{1-x}Ni_yAl_{1-y}O_3$. Revista Ciencia e Ingeniería, Vol. 38 (1), pp. 17-30.

Lugo, C., Rosal, H., Hidalgo, J., Rondón, J., Pérez, P., Rodríguez, P., Del Castillo, H. y Imbert, F., (**2022**). Preparation of single and layered Perovskites (A= La and Sr/Ca; B = Ni/Co and Ni/Al) from solution combustion synthesis, SCS, via microwave radiation. Revista Ciencia e Ingeniería, Vol. 43 (3), pp. 245-256.

Lugo C., Fereira C., Petit E., Guerrero M., Torres R., Pérez P., Rodríguez P., Rondón J., (**2024.a**). Estudio catalítico sobre RSM empleando óxidos mixtos Perovskitas $Sr_{0.7}Mg_{0.3}Ni_xCo_{1-x}O_3$, obtenidas vía combustión en solución, SCS. Revista Ciencia e Ingeniería, Vol. 45 (2), pp. 169-178.

Lugo C., Petit E., Guerrero M., Torres R., Fereira C., Pérez P., Rondón J., (**2024.b**). Síntesis de perovskitas en capas tipo $A_{n+1}B_nX_{3n+1}$ (A=Sr/Mg; B=Ni/Fe; X=O) vía SCS con Actividad Catalítica en el Reformado seco de metano. Revista Ciencia e Ingeniería, Vol. 45 (3), pp. 265-274.

Martín, N., Viniegra, M., Vargas, R., Garza, J., (**2021**). Óxidos nanoestructurados de metales de transición con aplicaciones en Catálisis. Mundo Nano, Vol. 14 (26), pp. 35-46.

Mukasyan, A., Costello, C., Sherlock, K., Lafarga, D., y Varma, A., (**2001**). Perovskite Membranes by Aqueous Combustion Synthesis: Synthesis and Properties. Separation and Purification Technology, Vol. 25 (1-3), pp. 117-126.

Mukasyan, A., Epstein, P. y Dinka, P., (**2007**). Solution combustion synthesis of nanomaterials. Proceedings of the Combustion Institute, Vol. 31 (2), pp. 1789-1795.

Neira, A., Gómez, J. y Vera, E., (**2016**). Synthesis and characterization of a simple $La_{0.8}Sr_{0.2}CrO_3$ perovskite

(Universidad del Valle). Revista de Ciencias, Vol. 20 (1), pp. 79-94.

Patil, K., Aruna, S. y Ekambaram, S., (**1997**). Combustion synthesis. Current Opinion in Solid State and Materials Science, Vol. 2 (2), pp. 158-165.

Patil, K., Aruna, S. y Mimani, T., (**2002**). Combustion synthesis: an update. Current Opinion in Solid State and Materials Science, Vol. 6 (6), pp. 507-512.

Pérez, M., Lugo, C., Quintero, M., Pérez, P., Villarroel, M., Rodríguez, P., Imbert, F. y Del Castillo, H., (**2015**). Síntesis de óxidos mixtos tipo perovskitas de $La_xSr_{1-x}Ni_yAl_{1-y}O_3$ preparados vía combustión en solución (SCS). Revista Ciencia e Ingeniería, Vol. 36 (2), pp. 93-104.

Rahdar, A., Aliahmad M., Azizi Y., (**2015**). NiO Nanoparticles: Synthesis and Characterization, Journal of Nanostructures, JNS, Vol. 5, 145-151.

Ramos, K., Jiménez, Y. y Linares C., (**2015**). Síntesis y caracterización de óxidos MgAl, MgFe, FeAl y MgFeAl para la degradación de fenol con foto-fenton solar. Revista latinoamericana de Metalurgia y Materiales, Vol. 35 (2), pp. 315-325.

Rendón, J., Moreno, L. y Valencia, J., (**2006**). Síntesis y caracterización de perovskitas de $LaCoO_3$ por el método citrato. Revista colombiana de Física, Vol. 38 (2), pp. 906-909.

Sierra, G., Gallego, J., Batiot-Dupeyrat, C., Barrault, J. y Mondragón, F., (**2009**). Influence of Pr and Ce in dry methane reforming catalysts produced from $La_{1-x}A_xNiO_{3-\delta}$ (A= Pr, Ce). Applied Catalysis A: General, Vol. 369, (1-2), pp. 97-103.

Sithole, M., Omondi, B., & Ndungu, P., (**2017**). Synthesis and characterization of $Ce_{0.6}Sr_{0.4}Fe_{0.8}Co_{0.2}O_{3-\delta}$ perovskite material: Potential cathode material for low temperature SOFCs. Journal of Rare Earths, Vol. 35 (4), pp. 389-397.

Song, S., Sheptyakov, D., Korsunsky, A., Duong, H. y Lu L., (**2016**). High Li ion conductivity in a garnet-type solid electrolyte via unusual site occupation of the doping Ca ions. Materials and Design, Vol. 93, pp. 232-237.

Specchia, S., Ciera, A. y Saracco, G., (**2004**). In situ combustion synthesis of perovskite catalysts for efficient and clean methane premixed metal burners. Chemical Engineering Science, Vol. 59 (22-23), pp. 5091-5098.

Varma, A., Mukasyan, A., Deshpande, K., Pranda, P. y Erii, P., (**2003**). Combustion Synthesis of Nanoscale Oxide Powders: Mechanism, Characterization and Properties. Materials Research Society Symposium Proceeding, Vol. 800, pp. 113-125.

Villaquirán, C., Medina, C., & Tirado, L., (**2015**). Effect of cobalt-incorporation on the proper-ties of $Sr_xBa_{1-x}Nb_2O_6$ system. Ingeniería y Desarrollo, Vol. 33 (2), pp. 281-300.

Wade L., (**2004**). Química Orgánica (quinta edición). Madrid-España: Pearson Educación S.A., 500, 505, 1207.

Wang, K., Zhong, P. y Zhu, J., (**2009**). Preparation of Highly Active and Stable Perovskite-like Catalyst by Combustion Method: Effect of Complex. Catalysis Letters, Vol. 131, pp. 672-675.

Zhao, Y., Hong, L., Hong, J. y Zhu, J., (**2004**). Synthesis of lead sulfide nanocrystals via microwave and sonochemical methods. Materials Chemistry and Physics, Vol. 87 (1), pp. 149-153.

Received: *May 22th, 2025*

Accepted: *July 17th, 2025*

Lugo González, Claudio Antonio: *Ph.D. in Applied Chemistry, mention Materials Studies, 2017, Universidad de Los Andes; Professor of Chemistry Department (Kinetics and Catalysis Laboratory), at the Faculty of Sciences, ULA. Merida, Venezuela.*

https://orcid.org/0000-0001-8003-0354

Guerrero Rojas, Maryuri: *Bachelor's Degree in Chemistry, 2023, Chemistry Department (Kinetics and Catalysis Laboratory) at the Faculty of Sciences, Universidad de Los Andes, Mérida, Venezuela. Email: mar94688@gmail.com*

https://orcid.org/0009-0000-8230-7038

Fereira Chacón, Carla Yanosky: *Bachelor's Degree in Chemistry, 2023, Chemistry Department (Kinetics and Catalysis Laboratory) at the Faculty of Sciences, Universidad de Los Andes, Mérida, Venezuela. Email: carlayanosky@gmail.com*

https://orcid.org/0009-0004-2961-7802

Petit Chacón, Eliel José: *Bachelor's Degree in Chemistry, 2023, Chemistry Department (Kinetics and Catalysis Laboratory) at the Faculty of Sciences, Universidad de Los Andes, Mérida, Venezuela. Email: elielpetit4@gmail.com*

https://orcid.org/0009-0004-3623-2732

Torres Ibarra Rubén Darío: *Bachelor's Degree in Chemistry, 2023, Chemistry Department (Kinetics and Catalysis Laboratory) at the Faculty of Sciences, Universidad de Los Andes, Mérida, Venezuela. Email: rubendti.16@gmail.com*

https://orcid.org/0009-0000-3600-8571

Vizcaya, Marietta: *Ph.D. in Drug Chemistry, 2014, Scientific Research Institute, Faculty of Pharmacy and Bioanalysis, Universidad de Los Andes; Professor of Polymer Laboratory at the Faculty of Sciences, ULA.*

Mérida, Venezuela. Email: marietta@ula.ve
https://orcid.org/ 0000-0002-2064-4175

Pérez Dávila, Patricia: *Ph.D. in Drug Chemistry, 2017, Scientific Research Institute, Faculty of Pharmacy and Bioanalysis, Universidad de Los Andes; Professor of Polymer Laboratory at the Faculty of Sciences, ULA. Mérida, Venezuela. Email: perezdpatricia@gmail.com*
https://orcid.org/0000-0003-0591-2351

Rondón Contreras, Jairo: *Ph.D. in Applied Chemistry, mention Materials Study, 2015, Universidad de Los Andes; Professor of Biomedical & Chemical Engineering Departments, at the Polytechnic University of Puerto Rico, San Juan, PR-USA. Email: jrondon@pupr.edu*
https://orcid.org/0000-0002-9738-966X